On outflow boundary conditions for CT-based computation of FFR: examination using PET images

Ernest WC Lo [1], Leon J Menezes [2] and Ryo Torii [3,*]

[1] UCL EPSRC CDT for Medical Imaging; Department of Medical Physics and Biomedical engineering, University College London; ernest.lo.15@ucl.ac.uk
[2] UCL Institute of Nuclear Medicine; NIHR University College London Hospitals Biomedical Research Centre; leon.menezes@nhs.net
[3] Department of Mechanical Engineering, University College London
* Correspondence: r.torii@ucl.ac.uk; Tel.: +44-20-7679-2801

Received: date; Accepted: date; Published: date

Abstract: CT-based computations of fractional flow reserve (FFR) have been widely utilized for evaluating functional severity of a coronary artery stenosis. Whilst this approach has been successful clinically, assumptions involved in the analysis still need to be investigated for further improvement of predictive accuracy. To better understand the sensitivity of computational FFRs on outflow boundary condition – typically reflecting patient's own physiology only through anatomical features – FFR computations for 10 patients with different degree of stenosis was conducted. The computations were based on 3D anatomical model reconstructed from CT images and patient-specific in/outflow boundary conditions (BC). Two outflow BCs were considered: (1) conventional morphology-based and (2) PET perfusion-based conditions. The results showed that the FFRs derived from the two boundary conditions agree in general. It was also found that the FFRs computed with the morphology-based BC tend to estimate higher functional severity, especially in patients with reduced vasodilatory response under hyperaemia – an essential physiological condition in FFR measurement. Further investigation was made by varying hyperaemic resistances (30%-90% of the baseline) in the morphology-based BC. The variation of FFR for the varied resistances was narrow for patients with mild stenosis and wider for those who have severe stenosis. This latter approach confirmed that variability of FFR due to outflow condition tends to come from overestimation of vasodilatory response, especially those who have abnormal myocardial perfusion. The results suggest that outflow conditions that are more representative of each patient could be an effective way to improve CT-based FFR computation.

Keywords: Coronary artery stenosis; CT-based FFR computation; outflow boundary conditions; positron emission tomography perfusion imaging

---

Highlights

- Computational FFR analysis was conducted using outflow conditions based on PET images to reflect myocardial perfusion in CFD.
- FFRs derived using conventional morphology-only-based outflow conditions (MBC) and PET-based conditions (PBC) agreed well.
- The difference of FFRs due to types of boundary condition is minimal for patients with mild stenosis and larger for those having a severe stenosis.
- The MBC with reduced peripheral resistance response generally explains the difference of FFR prediction due to poor myocardial perfusion.
- Additional model for poor vasodilatory response of patients with myocardial disease may improve the accuracy of the CT-based FFR computation.

1. Introduction

Coronary artery disease (CAD) is the single largest cause of death globally and accounts for 12% of annual deaths in the UK.[1] When coronary arteries are obstructed, it can lead to a mismatch between myocardial demand and supply for oxygen and nutrients, leading to failure of myocardial function, a state known as ischaemia.

In the clinical setting, the most common method to evaluate the severity of an obstruction involves X-ray coronary angiography, taking projection images of the arteries to determine the percentage of the diameter of the obstructed artery. However, for obstructions that are of an intermediate level, the predictive power of this approach for ischaemia is low and inter-observer variability is high, in the study by Fischer et al, using 3 observers, agreement on stenosis severity was as low as 55% and the overall concordance with FFR was about 50%.[2–4] This is because the ischaemic consequences of an obstruction does not only depend on the anatomical degree of obstruction, prompting the need of an indicator that assesses its functional severity.[5]

It was discovered that the severity of an obstructive stenosis can be determined by the ratio of maximum blood flow distal to a stenotic lesion to normal maximum flow in the myocardium. Practically, the ratio can be calculated by measuring the ratio between the distal and proximal pressures with respect to the stenosis.[6] This ratio is known as Fractional Flow Reserve (FFR). It has been demonstrated in the FAME 1 and FAME 2 trials that FFR is an effective diagnostic indicator in deciding the suitability of stent treatments.[7] FFR is measured during invasive coronary angiography where a pressure wire is inserted as part of catheterization to measure the blood pressure distal and proximal to the obstruction. The measurement takes place when the patient is in induced hyperaemia, under which blood flow across the coronary vasculature is maximized, usually by the administration of vasodilators such as adenosine.[6] The ratio of the pressures is defined as FFR and stenting is recommended when the FFR is lower than 0.8 that means the pressure distal to the obstruction is 80% of the pressure proximal. FFR is currently the gold standard for determining the severity of coronary artery obstructions.[8]

Computed Tomography Coronary Angiography (CTCA), has been more recently been pushed to the forefront of CAD diagnosis, due to its relatively lower cost and non-invasive procedure.[9] However, similarly to X-ray coronary angiography, CTCA only depicts the anatomical degree of obstruction rather than the functional severity. To address this limitation, FFRCT, also known as CT-based FFR or CT-FFR has been proposed [10], where 3D coronary artery anatomy obtained from CTCA is used in a computational fluid dynamics (CFD) simulation to calculate pressure in the vasculature. FFR can be obtained subsequently by assessing the computed pressure profile across a stenosis. CT-based FFR analysis for clinical diagnosis is gaining mainstream acceptance with various health governing bodies such as UK National Institute of Care and Excellence (NICE) recommending it as an diagnostic option, and the performance has been demonstrated in various clinical studies.[11–13] Effort has been made to further this technology, mostly to make it simplified for faster computation such as QFR[14], vFFR[15] and for the use with wider variety of imaging modality. Questions always arise however, with any simulation-based "measurements", regarding model assumptions, sensitivity to boundary conditions and input parameters.

A particular challenge is to model the behavior of the microvascular systems – vasodilation during the administration of vasodilators such as adenosine to induce hyperaemia in FFR measurements. Adenosine activates the A2A receptor causing coronary artery vasodilation, leading to 3.5 to 4-fold increase in myocardial flow in healthy humans.[16] The increase in flow under hyperaemia is known as coronary flow reserve (CFR), a functional measurement of coronary health similar but distinct to FFR. It reflects the health of an entire coronary tree including microvasculature whereas FFR only assesses the possibility of epicardial disease. In microvascular ischaemic disease, the vasodilatory response is reduced (a CFR of <2 is common in diseased patients) and in some extreme cases, adenosine causes no change from the resting state (CFR $\leq$ 1).[16] In simulation-based measurements, these microvessels are part of the downstream boundary conditions for the outflowing coronary branches, which are typically defined by the resistance of the microvessels. The ability of microvascular dilatation can thus have a significant influence on the flow

rate through each coronary branch. As CT cannot resolve microvascular behavior, many simulations resort to using this 4-fold increase of the flow as an assumption to adjust the downstream microvascular resistances for hyperaemic conditions.[10]

To tackle this challenge, we integrated CTCA and Positron Emission Tomography (PET) perfusion imaging into CT-based FFR measurements to realise simulations with outflow boundary conditions that are more patient-specific and representative of diseased coronary arteries. PET perfusion is currently the gold standard for assessing myocardial perfusion among available imaging modalities: SPECT, CT perfusion and MR perfusion.[17] Because PET myocardial perfusion imaging is performed on both rest and stressed states (i.e. normal and hyperaemia, respectively), it allows to incorporate a clear picture of how the microvasculature dilates in CT-based FFR simulation as outflow boundary conditions. In this pilot study using 10 patients' data, our aim was to examine the sensitivity of FFR to the types of outflow boundary conditions and evaluate the significance of patient-specific outflow boundary conditions. Additionally, a method to evaluate a potential range of FFR for individual patient is proposed and tested as an alternative method when perfusion is not known from PET or other type of imaging.

2. Materials and Methods

In this study, CFD analyses on 3D patient-specific anatomical models were conducted using various outflow boundary conditions: (1) structured tree boundary conditions with typical hyperaemic response (2) structured tree boundary conditions with hyperaemic response that is varied across the possible disease spectrum and (3) perfusion (PET) based boundary conditions.

2.1 Patients

This study included 10 patients (6 male, 4 female, age: 61.7$\pm$ 12.2 years) of various levels of angiographically determined epicardial stenosis (6 mild, 2 intermediate and 3 severe case). The patients presented chest pain and other symptoms that indicated an intermediate risk of coronary artery disease. All patients underwent 4D CTCA for anatomical assessment and ^{82}Rb PET perfusion imaging to identify ischaemic regions in the myocardium. Demographic details of the patients are summarised in Table 1. The study was carried out in accordance with the recommendations of the South East Research Ethics Research Committee (Aylesford, Kent, UK) with written informed consent from all subjects, in accordance with the Declaration of Helsinki.

The acquired ^{82}Rb PET perfusion images were processed in a custom-made MATLAB code to obtain local myocardial flow (details can be found in Supplemental materials A) and also in a clinical software platform (Syngo VB20A HF04) to obtain regional coronary flow reserve to be used as a reference in the analysis.

2.2 Image segmentation and meshing

CTCA images were segmented using Simpleware ScanIP (Synopsys, CA, USA) to produce 3-D anatomical models of the coronary arteries. Coronary branches were terminated at a diameter size above 2mm due to the resolution limit: 0.488 mm pixel size and 0.625 mm slice thickness. Meshing was performed also using ScanIP, using tetrahedral elements with 6 layers of prism elements along the boundaries, with total element number in the order of 10^6.

2.3 Blood flow computation

The blood flow in the anatomical models were computed by numerically solving the incompressible 3D Navier-Stokes equations using a commercial package ANSYS CFX 17.0 (ANSYS, Inc. Cannonsburg, USA). The flow was assumed to be laminar and blood was modelled as homogenous and Newtonian fluid with its density and dynamic viscosity 1060 kg/m^3 and 0.004 Pa s, respectively.

The vessel wall was approximated as rigid wall, where non-slip boundary conditions were applied, and cardiac-induced wall motion was not incorporated.

Table 1: Patient data table.

Patient	Sex	Age	Stenosed branch	Stenosis severity	
				Clinical classification	Diameter reduction on CT
1	M	79	RCA	intermediate	45%
2	M	59	LAD	mild	31%
3	F	64	LAD	severe	76%
4	F	75	LAD	mild	19%
5	F	80	RCA	severe	73%
6	M	51	LAD	trivial to mild	11%
7	F	64	LAD	trivial to mild	9%
8	M	50	RCA	mild	14%
9	M	50	RCA	trivial to mild	4%
10	M	45	LAD LCx	severe intermediate	55% 37%

RCA: right coronary artery, LAD: left anterior descending (artery), LCx: left circumflex.

2.4 Inflow boundary conditions

The inflow into the aorta was set as a steady flow. While this is not representative of ordinary cardiac function, a detailed comparison between steady and pulsatile flow conditions have shown that steady flow condition is sufficient in CT-based FFR calculations.[18] Inflows were set patient specific, calculated based on the difference between segmented ventricular cavity volume at maximum contraction in systole and maximum dilatation in diastole, multiplied by the patient's heart rate.

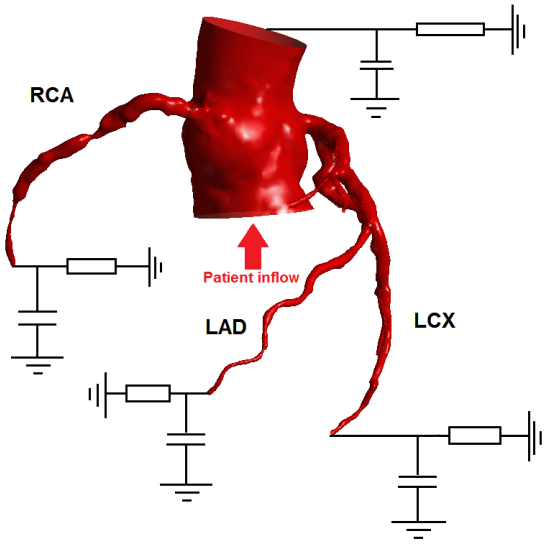

Figure 1. Schematic showing the outflow boundary conditions. All the boundary conditions are two-element Windkessel models represented in the circuit diagram.

2.5 Outflow boundary conditions

At each of the outflow boundaries, a two-element Windkessel model was connected to represent the downstream vasculature as shown in Figure 1. The Windkessel model is a 0D hydraulic-electric analogue where pressure difference, vascular resistance and compliance corresponds to potential difference, electrical resistance and capacitance.[19,20] The RC circuit is grounded to represent the near zero pressure conditions of the capillary bed. The model in practice provides pressure boundary conditions at each outlet in response to the outflow through the branch from the 3D CFD domain. Although the simulations were essentially steady state, we ran them as transient simulations with steady inflow, where compliance helps to stabilize the system and reach a steady state. The actual procedure to determine compliance values is explained in Section 2.5.1. There are many variations on the Windkessel model, such as the three-element, four-element and modified Windkessel, they are mostly used to simulate higher frequency phenomena in the cardiac cycle, which is irrelevant in a steady inflow simulation.[21]

In the baseline state, a reasonable assumption is to assign 5% of the total aortic output to the coronary arteries.[22] To accomplish this, the resistance at the aortic outlet was tuned such that the systemic outflow through the aorta corresponds to 95% of the stroke volume. In the hyperaemic state, however, the proportion of coronary flow to aortic output varies a lot more from patient to patient, and especially so in patients who suffer from some form of coronary artery disease. This was accounted for by adjusting peripheral resistance downstream to each branch, without control of the flow split between systemic and coronary circulations at hyperaemia. In conventional simulations in studies on coronary artery disease including CT-based FFR calculations, the assumption is made that the downstream resistance on the coronary branches is decreased to 30% of baseline[23], simulating the effect of adenosine inducing vasodilation.

2.5.1 Structured tree model for Windkessel outflow boundary conditions

To implement the conventional model of peripheral resistance, two parameters need to be calculated: the downstream resistance and vessel compliance. The resistances were determined using a structured tree model (Olufsen et al.[24]) to model a typical tree structure of small arteries and arterioles. This approach has been used effectively to supplement vessel tree structure beyond the resolution of CT (~0.5 mm) and has demonstrated to produce realistic resistance values for coronary flow simulations.[25] In practice, the branching structure of the vasculature and diameter of each segment (Figure 2) were defined using Murray's law[26] and empirical branch ratio 9:6 found in animal anatomy[24,25] following the equation below.

$$d_u^3 = d_{d1}^3 + d_{d2}^3$$

$$d_{d1} = \frac{a}{b} d_{d2}$$

Here, d_u is the diameter of the upstream or parent vessel in a bifurcation, d_{d1} and d_{d2} are diameters of as the two downstream or daughter vessels. Parameters a and b are branch ratio. The branching is repeated in a fractal-like manner until the limiting dimensions of an arteriole is reached, typically 0.05 mm in diameter. Once resistance is determined, vessel compliance was calculated by setting the time constant (=1/RC) equal to 0.063 s following the literature[27], although the compliance is unlikely to have a drastic effect on the simulation as the system converges to a steady state. Diameter at the beginning (proximal end) of the tree is equal to the diameter of 3D model at the peripheral end. In our study, baseline (not hyperaemic) resistance order of magnitude is ~ 100000 $dynes \cdot s \,/\, cm^2$

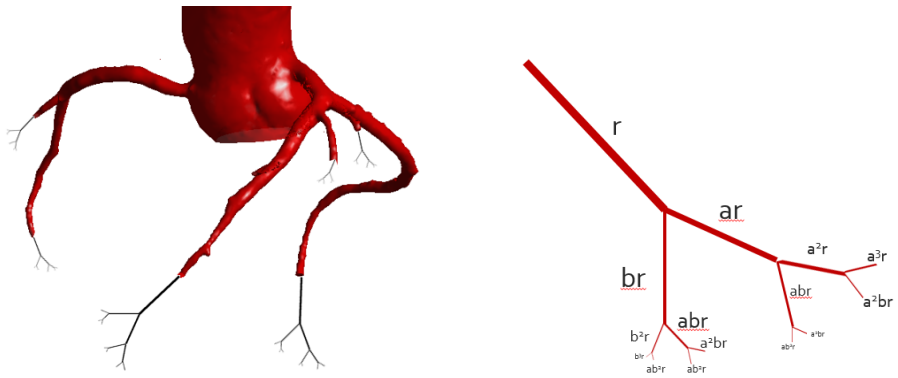

Figure 2: (Left) Illustration of downstream microvascular trees. (Right) Diagram of structured tree downstream microvascular structure. r represents the radius of the terminal vessel, and the daughter branches split asymmetrically in a repeated way, with fractions a and b, with values of 0.9 and 0.6 respectively.[24] This branching occurs indefinitely until it reaches the minimum radius.

2.5.2 Vasodilatory response model with structured tree

To test whether it is appropriate to set hyperaemic resistance to be 30% of baseline resistance and how sensitive FFR is to this, we performed simulations in which the downstream resistance of the diseased branch is adjusted to various reduced level (30%, 50%; 70%, 90%) of its baseline value calculated from the structural tree model. The range reflects the vast majority of patient disease cases, where microvascular vasodilatory response varies from healthy ideal to ineffectual (virtually no vasodilation). These conditions are referred as Morphological based Boundary Conditions (MBC) with their reduced resistance level, e.g. MBC 30%, MBC 50%, etc., later in the manuscript.

2.5.3 PET-based myocardial perfusion outflow boundary conditions

Because the CT and PET scans were not taken simultaneously though sequentially, co-registration is needed for the PET images to align with the correct myocardial region in the CT image. The PET images were first oversampled to produce the same pixel sizes as the CT images. Typically, the spatial resolution of CT was 0.5 mm/pixel (slice thickness 0.6mm) and that of PET image was 3 mm/pixel. The images were then aligned using a 5-point iterative closest point algorithm in Matlab, where 5 anatomical landmarks, such as the apex and basal end of the interventricular septum, are identified manually in both image sets and referred in the alignment. Co-registration uncertainty was calculated through 3 repeated attempts, which was found to be 1.74±0.40 mm within the transversal image plane and 2.71±0.55 mm out-of-plane (i.e. in the axis normal to the imaging plane).

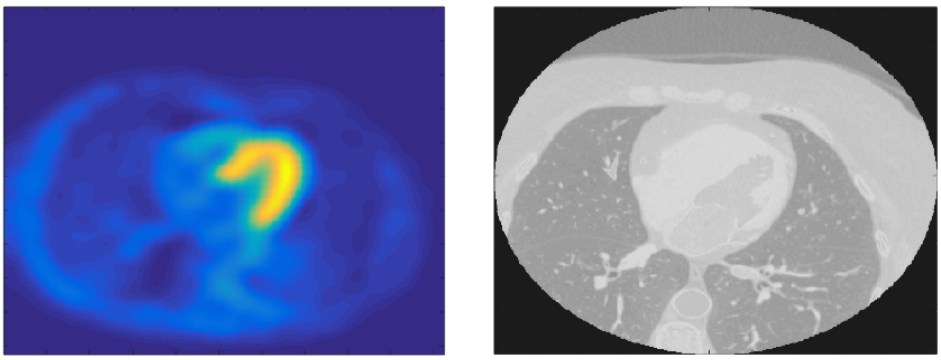

Figure 3: Typical PET image (left) and CT image (right) showing the long-axis slice of the heart. The colours in the PET image represents the spatial map of radiation intensity, corresponding to the myocardial perfusion. Here, the area of yellow-green indicates strong signal, depicting myocardium. The grayscale in the CT image corresponds to Hounsfield unit, the bright areas indicate regions of higher radiodensity.

A PET-perfusion-based boundary condition was developed to contrast the structured tree method which prescribes downstream resistances only based on the size of the of the branch terminus in the 3D model. The perfusion-based boundary condition (PBC) refers to the local perfusion quantitatively, based on the PET image intensity (representing perfusion in ml/100ml/min [16]), in the region supplied by each branch. Local perfusion was quantified by placing a sampling sphere (20 mm diameter) at the end of each branch in 3D model, and the special average of perfusion was calculated, excluding image pixels with its value lower than 10 ml/100ml/min in order to eliminate the space outside the myocardium in the sphere. The peripheral resistances downstream to each of the branches are then determined such that the flow split through each branch corresponds to the split in the PET-based measurement. Thus, in this approach, the resistance does not depend on the terminal branch size. Here, as in the MBC, the coronary outflow is assumed to be 5% of the total aortic output. A more detailed description of this process is presented in Supplemental material A.

Each patient has two sets of PET perfusion images, taken during the rest state (baseline) and during the hyperaemic state. The patient-specific and spatially local hyperaemic response can be calculated and implemented in the model, as a reduction of resistance so as to replicate the increased flow at hyperaemia in each branch. As the result, the total hyperaemic coronary outflow as a proportion of cardiac output is unbound and reflect the wide spectrum between patients.

2.6 Computational schemes

The governing equations are discretized in space using element-based finite volume method, where volume and surface integrations are performed at the Gaussian integration points on each element/face using tri-linear shape function interpolating nodal values of velocity and pressure in 3D within each element. The time integration was performed using 2nd order backward Euler scheme. Stabilization of the advection term is achieved by adaptive 2nd order upwinding scheme in which 1st order upwinding is blended with the 2nd order scheme in reference to the local flow velocity.

The simulations were carried out in quasi-steady condition, i.e. transient simulations were conducted with steady inflow boundary condition. This was required to account for the transient response of the downstream impedance. Here, the time step and convergence criteria were set to was set to 0.001 s and 1.0×10^{-5}, respectively. Sensitivity tests of the computational results to both mesh and time step size were carried out such that the pressure drop across a stenosis computed with the finally-chosen mesh and time step is less than 1% of difference compared to a mesh with doubled number of elements. Computations were conducted using 2 cores on standard desktop workstations (Intel Core i7 6700K 4GHz, 16GB RAM, 4 cores and Intel Xeon E5-2670 2.6GHz, 128GB RAM, 32 cores).

2.7 Calculation of FFR

Monitor points were placed at the coronary ostium and in the coronary artery at a point approximately 4 cm distal to the stenosis. FFR standards in invasive measurements specify at least 2-3 cm distally, 4 cm was chosen to be consistent and to ensure the minimum possible FFR (i.e. largest pressure drop in the vessel) is captured.[28] When the simulation has converged, the pressure distal to the stenosis divided by the pressure at the coronary ostium produces the final CT-based FFR value.

3. Results

Typical examples of the computational results, in terms of pressure distributions along the coronary vessel tree, are shown in Figure 4. Wide spectrum of anatomical variations and some different levels of pressure drop across the tree can be observed. The pressure drop from the aorta to the end of branches is in general larger for the models with PBC.

A quantitative comparison of FFR values across the stenosis is presented in Table 1, including those with all the peripheral resistance variations of MBC. FFR range is from 0.64 (Patient 5 with MBC 30%) to 0.99 (Patients 6 and 7 with PBC). In reference to the cut-off value of CT-based FFR (0.80 [29]), the range of FFR in this study reflects the wide range of disease state included in the study.

The FFR with PBC and 'the standard (i.e. 30%)' MBC are in general correlated well (r = 0.68). The correlation is higher for the patients with high FFR values (FFR >> 0.80), i.e. patients with relatively minor or insignificant stenosis. The PBC tends to result in FFRs that are higher than the ones with the conventional boundary condition (MBC 30%). However, this is not true for Patients 3, 9 and 10. Patient 3 is the most extreme case where the FFR with PBC (0.76) indicates a different diagnostic result than the conventional MBC 30% (FFR=0.81), straddling across the standard cut-off value of 0.80.[29]

The FFR values obtained with the variable peripheral resistances in MBC show a clear trend of high FFR for high resistance (i.e. smaller degree of resistance reduction – close to the baseline) consistently across the patients. This was expected, based on a principle of fluid mechanics; low peripheral resistance invites higher flow to the branch which results in a larger pressure drop thus smaller FFR.

The flow rates through different branches are summarised in Table 3, both in absolute value and proportion to the total coronary flow. A comparison between Tables 2 and 3 indicates that the flow rate is a strong determinant of FFR, with higher flow rates corresponding to lower FFR (more severe stenosis). Considering Poisuelle's law, the flow rate increase should linearly be related to the pressure drop (1 – FFR gives the pressure drop as a proportion of proximal pressure), which is also true in these vessels. Additionally, the MBCs with various level of peripheral resistance demonstrate a strong association between the flow rate and the percentage of coronary flow that is distributed to the stenotic branch. In general, the flow through the stenosed branch is lower with PBC than with MBC but for Patients 3, 9 and 10 (LCx), where the PBC-based FFR was lower than that of MBC 30%, the flow with PBC is indeed higher.

Figure 5 is a graphical representation of Table 2, showing FFRs obtained with PBC and MBC with the range of reduced peripheral resistance. Here, the range of FFR with the variable MBC is examined in a different way to illustrate more fundamental principle underpinning their relationship. The patients are reordered in reference to FFR with MBC 30% so that the trend is clearly visible. For patients with an FFR close to or below the cutoff of 0.8, the divergence in FFR values between PBC and MBC 30% is more significant. The range of FFR for the various peripheral resistance is also larger for the lower overall FFR. On the other hand, the range for patients having high overall FFR is small, only 0.01 for Patients 4, 7 and 9.

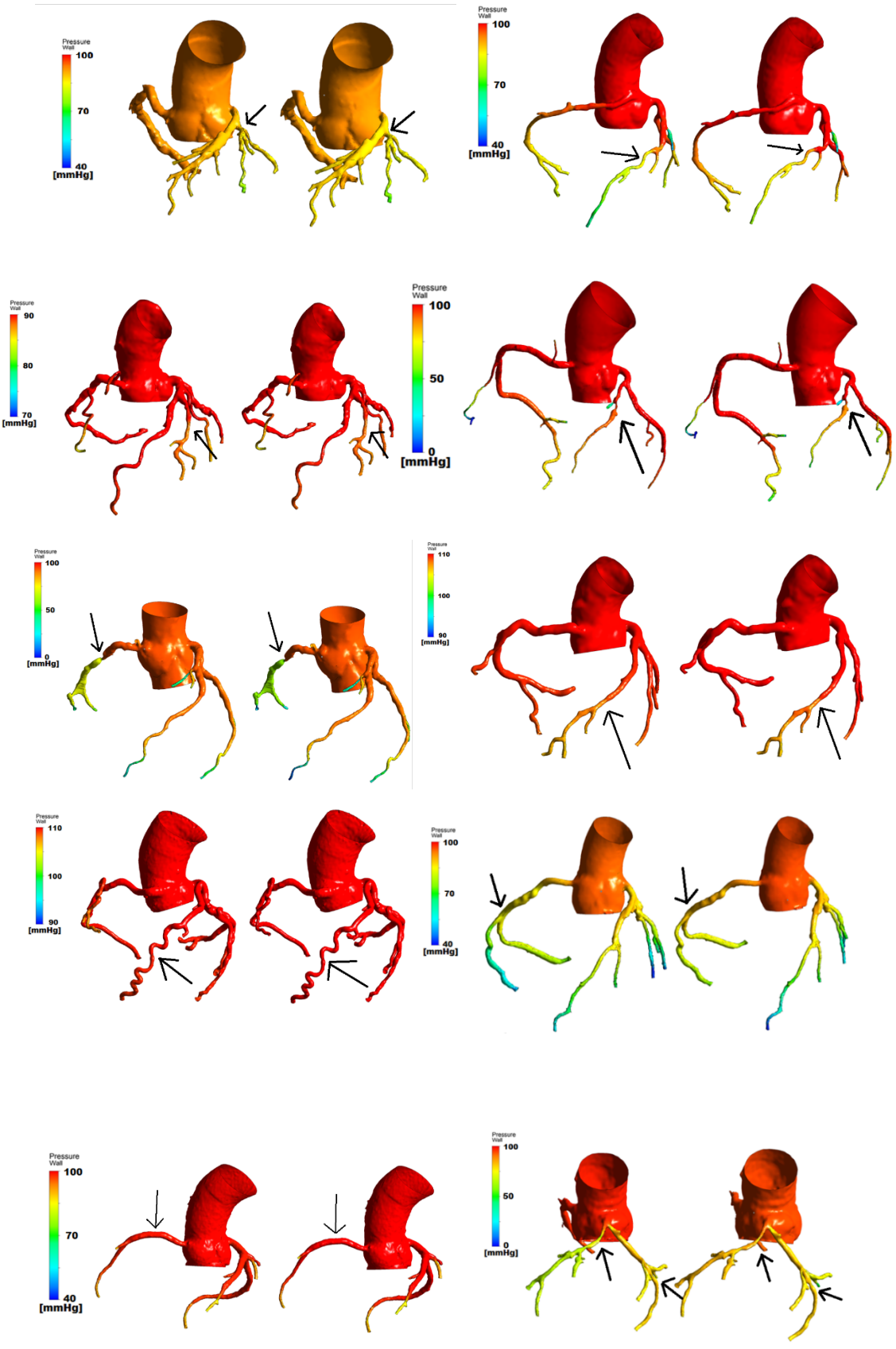

Figure 4: Comparison of pressure profiles obtained from PET-based boundary conditions (left of pairs) versus conventional morphology-based boundary conditions (right of pairs). Patient 1-10 from top left to the bottom right. Arrows indicate focal stenosis.

Table 2. CT-based FFR values obtained using various outflow boundary conditions. PBC: PET-based boundary condition, MBC: morphology-based boundary condition. The percentage values indicate reduced resistance level to account for hyperaemic flow increase and reduction to 30% (MBC 30%) is the conventional assumption.

Patient	PBC	MBC (30%) "Conventional"	MBC (50%)	MBC (70%)	MBC (90%)
1	0.91	0.89	0.91	0.92	0.92
2	0.90	0.83	0.88	0.92	0.93
3	0.76	0.81	0.83	0.84	0.85
4	0.97	0.96	0.96	0.97	0.97
5	0.71	0.64	0.74	0.75	0.75
6	0.99	0.96	0.96	0.98	0.99
7	0.99	0.97	0.98	0.98	0.98
8	0.85	0.82	0.85	0.86	0.88
9	0.96	0.98	0.98	0.98	0.99
10 (LAD)	0.73	0.56	0.68	0.74	0.78
10 (LCx)	0.74	0.77	0.85	0.88	0.88

Table 3. Flow rates through stenosis and proportion of that to the overall coronary flow (%), obtained using various outflow boundary conditions.

Patient	PBC, [ml/s]	MBC (30%), [ml/s]	MBC (50%), [ml/s]	MBC (70%), [ml/s]	MBC (90%), [ml/s]
1	3.98 (48%)	4.69 (56%)	3.78 (45%)	3.39 (41%)	3.26 (39%)
2	3.41 (40%)	5.54 (64%)	4.59 (53%)	2.72 (32%)	2.50 (29%)
3	2.78 (29%)	2.23 (28%)	2.07 (26%)	1.82 (23%)	1.74 (22%)
4	2.61 (32%)	3.45 (38%)	2.87 (32%)	2.57 (29%)	2.42 (27%)
5	1.39 (20%)	1.72 (22%)	1.28 (16%)	1.26 (16%)	1.20 (15%)
6	2.19 (33%)	5.18 (68%)	4.37 (57%)	2.79 (37%)	1.45 (19%)
7	1.34 (17%)	2.86 (22%)	2.35 (18%)	2.11 (16%)	1.98 (15%)
8	1.69 (16%)	2.14 (21%)	1.71 (17%)	1.52 (15%)	1.32 (13%)
9	5.01 (55%)	4.50 (53%)	4.12 (48%)	3.90 (46%)	2.56 (30%)
10 (LAD)	2.24 (21%)	3.83 (34%)	2.82 (25%)	2.17 (19%)	1.91 (17%)
10 (LCx)	1.22 (11%)	1.09 (9.5%)	0.71 (6.2%)	0.58 (5.1%)	0.56(4.9%)

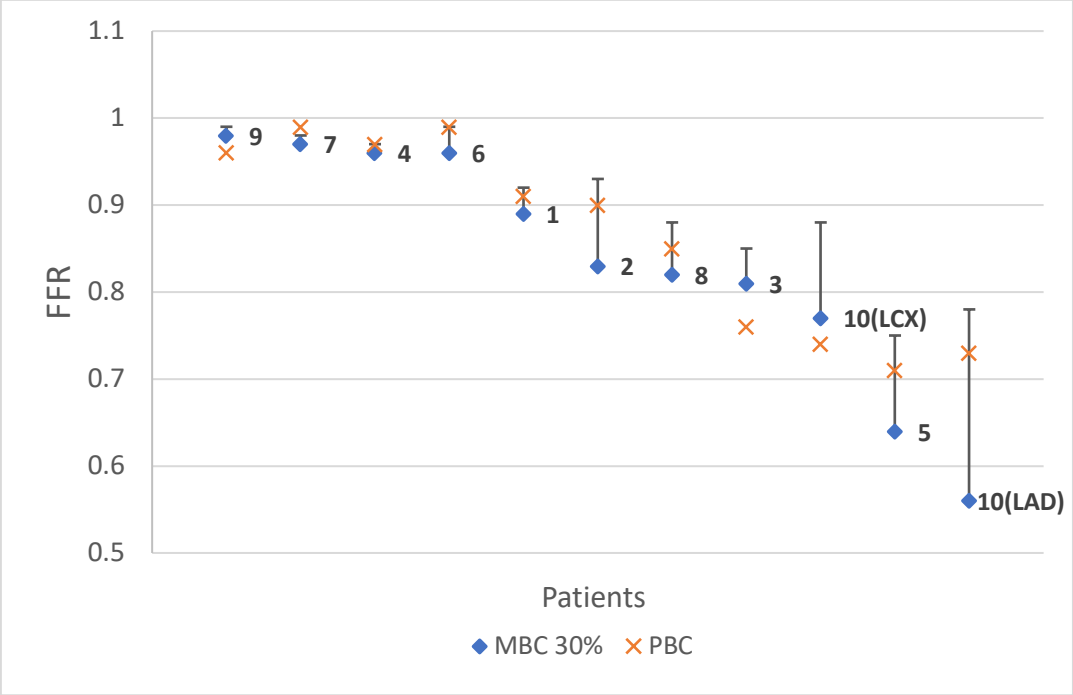

Figure 5: The FFRs of patients, reordered in reference to the value of FFR calculated with MBC 30%. The bars indicate the range of FFRs obtained using the various MBCs, with the conventional (MBC 30%) marked as a blue diamond, and the PBC marked as orange cross. Patient numbers are shown on the plot as reference.

4 4. Discussion

Although coronary artery flow computations have relatively long history and boundary conditions have always been a point of discussion, to the authors' knowledge, there was no study utilising myocardial perfusion as patient-specific outflow conditions. The perfusion data was used to examine the impact of resistance reduction during hyperaemia, and an attempt was made to characterise an uncertainty range of FFR due to non-ideal response to vasodilator by the vasculature peripheral to the stenosis. Uncertainty of FFR computation has been studied in terms of the sensitivity of FFR to imaging and segmentation uncertainty[29], but not the hyperaemic response to adenosine.

The results show a high correlation of FFR values computed using the two types of outflow boundary conditions. This is not surprising for the patients with relatively minor stenosis because there is no significant pressure drop across the stenosis anyways. Therefore, even with different flow distributions across the branches of the coronary arteries obtained via the varied outflow boundary conditions, the pressure drop across the stenosis for those patients was not significantly altered (e.g. Patient 9, FFR range: 0.98-0.99 for various MBCs).

On the other hand, the hyperaemic condition is shown to have a strong influence on the FFR calculations for more severe stenosis such as Patients 3, 5 and 10. The pressure drop ΔP across a flow limiting pipe is related to its flow rate Q and resistance R (in this case, the stenosis): $\Delta P \approx Q \times R$, using Poiseuille's law. An increase in flow rate for a given stenosis increases the pressure drop, and Similarly, a more severe stenosis (i.e. increased resistance) increases the pressure drop, therefore lowering FFR. This is a simple fluid mechanical principle behind the differences caused in FFR. The same principle also implies that a reduced flow rate in a stenosis would result in a higher FFR, i.e. indication for a less functional severity. A reduced flow can occur if there is any disease in the peripheral vascular bed (microvascular disease), which could elevate FFR. From diagnostic point of view, this may appear to be false negative scenario, i.e. diseased patient seen as healthy. However,

the purpose of FFR is to detect a focal flow-limiting stenosis, and a relatively high FFR indicating the stenosis being no flow-limiting in such a scenario still provides a valid indication.

The simulations using the PET perfusion-based boundary conditions take into account the patient-specific distribution of the flow across the different branches and the change in flow rate from normal physiological state to hyperaemia. The FFR obtained using the PBCs are in general higher than the FFRs with conventional boundary conditions. This is because the hyperaemic response in reality is generally less than 4 with a wide range standard deviation of 0.9)[16] and the PET perfusion boundary conditions reflect that. Clinically-evaluated CFRs of our patients' diseased vessels are 2.12±1.28, indicating that the conventional assumption, i.e. CFR=4, is indeed an overestimate. However, in Patients 3 and 10, the FFR values obtained using PBC are lower than those using MBC. Even though the conventional boundary conditions make the assumption of the ideal vasodilatory condition (4x the baseline flow), the baseline flow for the diseased branch may be higher in the model with PBC than with MBC, and therefore even with a reduced vasodilatory condition with PBC (<4x), the absolute hyperaemic flow across the diseased branch can be higher than that of the conventional model as shown in Table 3, causing a larger pressure drop and hence lower FFR. This is indeed true for those 2 patients, suggesting that the myocardium downstream to those vessels are still healthy despite the stenosis in its upstream, making these cases as illustrative examples of 'flow-limiting' stenosis that should ideally be detected by FFR. The flow through the diseased branch of those patients are underestimated with the conventional MBC, thus potentially causing false negative – indeed, the FFR of MBCs are higher than the cutoff 0.8 and that with PBC is lower. To make the analysis framework more accurate, this group of patients need to be looked at for further characterisation.

The PBC-based FFRs generally fall within the range of FFR calculated using the varied MBC (30%-90%). The patients where the PET perfusion model predicts an FFR that is outside the bounds all have a higher flow through the stenosed branch compared to the computations with MBC. The method of ranging the hyperaemic response to obtain a lower and upper bound of FFR could therefore be useful approach to have a 'confidence interval' of FFR calculation. From clinical diagnostic point of view, it is particularly concerning when the range of FFR for a particular patient's stenosis straddles the cutoff value 0.9. The largest variance in FFR can be found in Patient 10, specifically with the LAD (0.56-0.78), however the bounds do not cross over the cut off and therefore it is unlikely to affect clinical decisions. For the LCx of Patient 10, while the variance is not as high, the range is across the clinical cutoff of 0.8 (0.74 – 0.88).

It should be noted that PET perfusion or other similar myocardial perfusion imaging generally supplants FFR measurement obtained both invasively or non-invasively.[31] It is rare in the clinic that both of those are performed before a diagnostic judgement is made, due to the cost and time it requires. The comparison in this study is not to suggest that a perfusion-based CT-FFR model should be adopted as clinical practice, but rather verifying the flow condition estimation in the downstream of the coronary arteries using purely morphological methods. That being said, there have been clinical studies that implement myocardial perfusion imaging in cases where CT-FFR provided an ambiguous indication, and has shown a noticeable improvement in diagnostic accuracy.[32]

Among patients having stable angina, 65% of women and 32% of men have no obstructive CAD (stenosis <50%).[33] A significant portion of those patients suffer from coronary microvascular dysfunction which can be ischaemia without a focal stenosis[33]. This means that a significant number of patients would not be best served by current CT-based FFR techniques that make the assumption of ideal downstream microvascular health. Because the assumption uses the maximal possible vasodilation, for patients whose vasodilatory response is impaired, the simulation would overestimate the flow passing through a stenosis, producing a lower FFR than the true value, potentially leading to false positive diagnosis and hence an unnecessary invasive revascularization.

Although the FAME trials – the original and main clinical trial for FFR – suggest a strict 0.8 cutoff, research has since suggested that clinicians should be cognizant of the biological variability of FFR measurements, where repeated measurements will produce different values and possibly

different diagnostic outcomes. [34] It has been suggested that there should be a gray zone around the cutoff, considered to be between 0.75 and 0.85, with particular caution given to values between 0.77 and 0.83, where the clinician will need to consider other patient metrics before deciding treatment.[34]. This study has examined one major consideration that can have a drastic effect on CT-based FFR: the vasodilatory capacity of the patient's microvessels. The PET perfusion-based model has shown that the majority of patient's microvascular health is between ideal and diseased, based on their CFR. In the clinic, additional assessment of microvascular health through testing or identifying risk factors such as diabetes, age, sex could be used to inform CT-based FFR measurements directly, producing a possibly more reliable FFR value, and if that isn't available, a similar approach to this study where a band of FFR values can be produced to identify the likelihood that a stenosis falls below the cutoff.

5. Limitations

The main limitation of this study is that the CT-based FFR values for the patients were not validated against invasive FFR, the gold standard for FFR. This preliminary study was designed as a sensitivity test, examining the variability of FFR in simulation-based CT-FFR with various outflow boundary conditions. Additionally, diffuse disease, where the narrowing isn't focal but spread along an artery, is also a known cause of ischaemia, and the pressure drops can be as severe as those of focal stenoses, however revascularization of diffuse disease has shown mixed results and therefore FFR is not applicable[35]. Model assumptions, not only with boundary conditions, are inevitable in computational analysis. We chose to simulate the flows with steady flow condition using Newtonian approximation of the blood. As discussed in method section, these are not deeded significant in FFR computation but would carry more importance in analyses of stented segment with potentially larger flow recirculation, and/or of patients with cardiac rhythm disorders. Lastly, the finding from our study still need to be confirmed with a larger number of patients, which is planned for future.

6. Conclusions

In this study, a series of computational FFR analysis was conducted using various outflow boundary conditions to investigate their impact on the FFR derivation. The FFRs computed with a conventional morphology-based and the novel PET-based outflow boundary conditions agreed in general. However, the models with PET-based condition revealed that there are cases in which conventional boundary condition overestimate the functional severity of a stenosis, potentially placing the patient in different diagnostic category. The derivation of a potential range of FFR a patient might have, by varying peripheral resistance over a physiologically possible range, indeed indicated that the overestimation of vasodilatory response is likely reason behind the overestimation of functional severity. These results indicate that, although perfusion data such as PET images are not always available in clinics, a better estimation of outflow boundary condition reflecting the physiological state of downstream coronary vasculature could improve the CT-based estimation of FFR.

Acknowledgements: This work is supported by the EPSRC-funded UCL Centre for Doctoral Training in Medical Imaging (EP/L016478/1) and the Department of Health's NIHR-funded Biomedical Research Centre at University College London Hospitals. The authors acknowledge Mr Raymond Endozo (Nuclear Medicine, UCL Hospital) for his help on data collection.

Supplemental material A

The PET perfusion measurement works as follows:

1. Generate a sphere of 20 mm diameter around the terminal end of a coronary branch (this has to be located using the CT image during segmentation) in the 3D model. The sphere in general overlaps significantly with the myocardial region supplied by the chosen coronary branch.

2. Sample the sphere for perfusion values above 10 ml/100ml/min (a normal value of perfusion is between 50 – 300ml/100ml/min[16]), effectively ruling out the spaces captured in the sphere where it is outside the myocardium.

3. Calculate the spatial mean perfusion of the myocardial region within the sphere, this value is used to represent the flow capacity of a coronary branch.

4. In the baseline (resting state) simulation, the 5% of aortic output that is allocated to the coronaries is divided by the various branches via their flow capacities, that are implemented in the form of downstream microvascular resistance.

5. In the hyperaemic (stressed state) simulation, the magnitude decrease in resistance of each branch is derived from the change in perfusion that is observed between the rest and stressed states.

The 20mm sphere size was chosen to be large enough to mitigate the problems that may arise from the registration error of 2-3mm, mis-identification of the location of the terminal end (usually due to CT resolution terminating branch far too proximal), and small enough that the regional perfusion supplied by different branches do not overlap significantly.

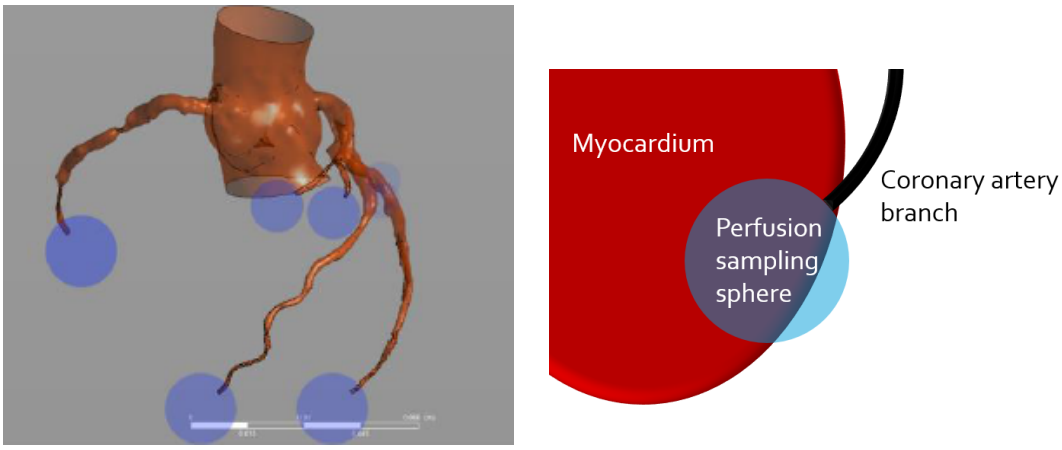

Figure A1: *Perfusion sampling spheres at the downstream terminus of coronary artery branches (left). The overlapping volume between sampling sphere and myocardium is used to quantify the local perfusion (right).*

Supplemental material B

Patient 10 has two significant stenosis on two separate branches, the LAD and LCx. In order to examine potential interaction of the flow in the two branches under the varied peripheral resistances, we varied the hyperaemic condition first in each of the LAD and LCx individually, and then both LAD/LCx simultaneously. The result is summarised in Table B1, it is observed that though the FFR values one branch are affected by the varying outflow condition of other branches, the effect is minor.

Therefore, the effect of varying peripheral resistance in two stenosed branches can practically be seen as independent.

Table B1. CT-based FFR values for Patient 10 when each diseased vessel's hyperaemic condition were varied individually and in combination.

Branch with varied BC	MBC 30%	MBC 50%	MBC 70%	MBC 90%
LAD	(LAD) 0.56 (LCx) 0.77	(LAD) 0.68 (LCx) 0.77	(LAD) 0.74 (LCx) 0.76	(LAD) 0.78 (LCx) 0.76
LCx	(LAD) 0.56 (LCx) 0.77	(LAD) 0.56 (LCx) 0.85	(LAD) 0.56 (LCx) 0.88	(LAD) 0.55 (LCx) 0.88
LAD+LCx	(LAD) 0.56 (LCx) 0.77	(LAD) 0.65 (LCx) 0.86	(LAD) 0.73 (LCx) 0.89	(LAD) 0.76 (LCx) 0.90

References

[1] Bhatnagar P, Wickramasinghe K, Williams J, et al. The epidemiology of cardiovascular disease in the UK 2014. Heart 2015;101:1182-1189.

[2] Montalescot G, Sechtem U, Achenbach S, Andreotti F, Arden C, Budaj A, et al. 2013 ESC guidelines on the management of stable coronary artery disease - addenda. Eur Heart J 2013;34:2949–3003. doi:10.1093/eurheartj/eht296.

[3] Hachamovitch R, Hayes SW, Friedman JD, Cohen I, Berman DS. Comparison of the short-term survival benefit associated with revascularization compared with medical therapy in patients with no prior coronary artery disease undergoing stress myocardial perfusion single photon emission computed tomography. Circulation 2003;107:2900–6. doi:10.1161/01.CIR.0000072790.23090.41.

[4] Fischer JJ, Samady H, McPherson JA, Sarembock IJ, Powers ER, Gimple LW, et al. Comparison between visual assessment and quantitative angiography versus fractional flow reserve for native coronary narrowings of moderate severity. Am J Cardiol 2002;90:210–5. doi:10.1016/S0002-9149(02)02456-6.

[5] Pim A.L. Tonino, M.D., Bernard De Bruyne, M.D., Ph.D., Nico H.J. Pijls, M.D. PD, Uwe Siebert, M.D., M.P.H., Sc.D., Fumiaki Ikeno, M.D., Marcel van 't Veer, M.Sc., Volker Klauss, M.D., Ph.D., Ganesh Manoharan, M.D., Thomas Engstrøm, M.D., Ph.D., Keith G. Oldroyd, M.D., Peter N. Ver Lee, M.D., Philip A. MacCarthy, M.D., Ph.D., and Willi MD. Fractional Flow Reserve versus Angiography for Guiding Percutaneous Coronary Intervention Pim. Sci York 2006:2213–24. doi:10.1056/NEJMoa1109400.

[6] De Bruyne B, Sarma J. Fractional flow reserve: a review. Heart 2008;94:949–59. doi:10.1136/hrt.2007.122838.

[7] Heyndrickx GR, Tóth GG. The FAME Trials: Impact on Clinical Decision Making. Interv Cardiol Rev 2016;11:116. doi:10.15420/icr.2016:14:3.

[8] Van Nunen LX, Zimmermann FM, Tonino PAL, Barbato E, Baumbach A, Engstrøm T, et al. Fractional

flow reserve versus angiography for guidance of PCI in patients with multivessel coronary artery disease (FAME): 5-year follow-up of a randomised controlled trial. Lancet 2015;386. doi:10.1016/S0140-6736(15)00057-4.

[9] Moss AJ, Williams MC, Newby DE, Nicol ED. The Updated NICE Guidelines: Cardiac CT as the First-Line Test for Coronary Artery Disease. Curr Cardiovasc Imaging Rep 2017;10. doi:10.1007/s12410-017-9412-6.

[10] Zarins CK, Taylor CA, Min JK. Computed fractional flow reserve (FFTCT) derived from coronary CT angiography. J Cardiovasc Transl Res 2013;6:708–14. doi:10.1007/s12265-013-9498-4.

[11] HeartFlow FFRCT for estimating fractional flow reserve from coronary CT angiography | NICE Guidance and guidelines | 2017.

[12] Taylor CA, Fonte TA, Min JK. Computational fluid dynamics applied to cardiac computed tomography for noninvasive quantification of fractional flow reserve: Scientific basis. J Am Coll Cardiol 2013;61:2233–41. doi:10.1016/j.jacc.2012.11.083.

[13] Taylor CA, Gaur S, Leipsic J, Achenbach S, Berman DS, Jensen JM, et al. Effect of the ratio of coronary arterial lumen volume to left ventricle myocardial mass derived from coronary CT angiography on fractional flow reserve. J Cardiovasc Comput Tomogr 2017;11:429–36. doi:10.1016/j.jcct.2017.08.001.

[14] Tu S, Westra J, Yang J, von Birgelen C, Ferrara A, Pellicano M, et al. Diagnostic Accuracy of Fast Computational Approaches to Derive Fractional Flow Reserve From Diagnostic Coronary Angiography. JACC Cardiovasc Interv 2016;9:2024–35. doi:10.1016/j.jcin.2016.07.013.

[15] Masdjedi K, Van Zandvoort L, Balbi M,et al. Validation of 3-Dimensional Quantitative Coronary Angiography based software to calculate vessel-FFR (the FAST study)., EuroPCR; 2018.

[16] Sdringola S, Johnson NP, Kirkeeide RL, Cid E, Gould KL. Impact of Unexpected Factors on Quantitative Myocardial Perfusion and Coronary Flow Reserve in Young, Asymptomatic Volunteers. JACC Cardiovasc Imaging 2011;4:402–12. doi:10.1016/J.JCMG.2011.02.008.

[17] Lortie M, Beanlands RSB, Yoshinaga K, Klein R, DaSilva JN, deKemp RA. Quantification of myocardial blood flow with 82Rb dynamic PET imaging. Eur J Nucl Med Mol Imaging 2007;34:1765–74. doi:10.1007/s00259-007-0478-2.

[18] Morris PD, van de Vosse FN, Lawford P V., Hose DR, Gunn JP. "Virtual" (Computed) Fractional Flow Reserve. JACC Cardiovasc Interv 2015;8:1009–17. doi:10.1016/j.jcin.2015.04.006.

[19] Sagawa K, Lie RK, Schaefer J. Translation of Otto frank's paper "Die Grundform des arteriellen Pulses" zeitschrift für biologie 37: 483–526 (1899). J Mol Cell Cardiol 1990;22:253–4. doi:10.1016/0022-2828(90)91459-K.

[20] Westerhof N, Lankhaar JW, Westerhof BE. The arterial windkessel. Med Biol Eng Comput 2009;47:131–41. doi:10.1007/s11517-008-0359-2.

[21] Francis SE. Continuous Estimation of Cardiac Output and Arterial Resistance from Arterial Blood Pressure using a Third-Order Windkessel Model (Master's Thesis) 2007.

[22] Ramanathan T, Skinner H. Coronary blood flow. Contin Educ Anaesthesia, Crit Care Pain 2005;5:61–4. doi:10.1093/bjaceaccp/mki012.

[23] Wilson RF, Wyche K, Christensen B V, Zimmer S, Laxson DD. Clinical Investigation Effects of Adenosine on Human Coronary Arterial Circulation. Circulation 1990;82:1595–606. doi:10.1161/01.CIR.82.5.1595.

[24] Olufsen MS. Structured tree outflow condition for blood flow in larger systemic arteries. Am J Physiol Circ Physiol 1999;276:H257–68. doi:10.1152/ajpheart.1999.276.1.H257.

[25] Olufsen MS, Peskin CS, Kim WY, Pedersen EM, Nadim A, Larsen J. Numerical simulation and experimental validation of blood flow in arteries with structured-tree outflow conditions. Ann Biomed Eng 2000;28:1281–99. doi:10.1114/1.1326031.

[26] Murray CD. The Physiological Principle of Minimum Work : I. The vascular system and the cost of blood volume. Proc Natl Acad Sci U S A 1926;12:207–14. doi:10.1085/jgp.9.6.835.

[27] Kim HJ, Vignon-Clementel IE, Coogan JS, Figueroa CA, Jansen KE, Taylor CA. Patient-specific modeling of blood flow and pressure in human coronary arteries. Ann Biomed Eng 2010;38:3195–209. doi:10.1007/s10439-010-0083-6.

[28] Solecki M, Kruk M, Demkow M, Schoepf UJ, Reynolds MA, Wardziak Ł, et al. What is the optimal anatomic location for coronary artery pressure measurement at CT-derived FFR? J Cardiovasc Comput Tomogr 2017;11:397–403. doi:10.1016/j.jcct.2017.08.004.

[29] Sankaran S, Kim HJ, Choi G, Taylor CA. Uncertainty quantification in coronary blood flow simulations: Impact of geometry, boundary conditions and blood viscosity. J Biomech 2016;49:2540–7. doi:10.1016/j.jbiomech.2016.01.002.

[31] Takx RAP, Blomberg BA, Aidi H El, Habets J, De Jong PA, Nagel E, et al. Diagnostic Accuracy of Stress Myocardial Perfusion Imaging Compared to Invasive Coronary Angiography With Fractional Flow Reserve Meta-Analysis 2015:1–7. doi:10.1161/CIRCIMAGING.114.002666.

[32] Coenen A, Rossi A, Lubbers MM, Kurata A, Kono AK, Chelu RG, et al. Integrating CT Myocardial Perfusion and CT-FFR in the Work-Up of Coronary Artery Disease. JACC Cardiovasc Imaging 2017;10:760–70. doi:10.1016/j.jcmg.2016.09.028.

[33] Alrifai A, Kabach M, Nieves J, Pino J, Chait R. Microvascular Coronary Artery Disease: Review Article. US Cardiol Rev 2017:1. doi:10.15420/usc.2017:27:1.

[34] Petraco R, Sen S, Nijjer S, Echavarria-Pinto M, Escaned J, Francis DP, et al. Fractional Flow Reserve–Guided Revascularization: Practical Implications of a Diagnostic Gray Zone and Measurement Variability on Clinical Decisions. JACC Cardiovasc Interv 2013;6:222–5. doi:10.1016/J.JCIN.2012.10.014.

[35] Gould KL, Johnson NP. Coronary Physiology Beyond Coronary Flow Reserve in Microvascular Angina:

624 JACC State-of-the-Art Review. J Am Coll Cardiol 2018;72:2642–62. doi:10.1016/j.jacc.2018.07.106.

625